

Asymmetry in the current sheet and secondary magnetic flux ropes during guide field magnetic reconnection

Rongsheng Wang,¹ Rumi Nakamura,¹ Quanming Lu,² Aimin Du,³ Tielong Zhang,¹ Wolfgang Baumjohann,¹ Yuri V. Khotyaintsev,⁴ Martin Volwerk,¹ Mats André,⁴ M. Fujimoto,⁵ T. K. M. Nakamura,⁵ Andrew N. Fazakerley,⁶ Jian Du,⁷ Waileong Teh,¹ Evgeny V. Panov,¹ Bertalan Zieger,^{1,8} Yongxin Pan,³ and San Lu²

Received 17 November 2011; revised 10 June 2012; accepted 19 June 2012; published 31 July 2012.

[1] A magnetic reconnection event with a moderate guide field encountered by Cluster in the near-Earth tail on 28 August 2002 is reported. The guide field points downward during this event. The quadrupolar structure of the Hall magnetic field within the ion diffusion region is distorted toward the northern hemisphere in the earthward part while toward the southern hemisphere tailward part of X-line. Observations of current density and electron pitch angle distribution indicate that the distorted quadrupolar structure is formed due to a deformed Hall electron current system. Cluster crossed the ion diffusion region from south to north earthward of the X-line. An electron density cavity is confirmed in the northern separatrix layer while a thin current layer (TCL) is measured in the southern separatrix layer. The TCL is formed due to electrons injected into the X-line along the magnetic field. These observations are different from simulation results where the cavity is produced associated with inflow electrons along the southern separatrix while the strong current sheet appears with the outflow electron beam along the northern separatrix. The energy of the inflowing electron in the separatrix layer could extend up to 10 keV. Energetic electron fluxes up to 50 keV have a clear peak in the TCL. The length of the separatrix layer is estimated to be at least $65 c/\omega_{pi}$. These observations suggest that electrons could be pre-accelerated before they are ejected into the X-line region along the separatrix. Multiple secondary flux ropes moving earthward are observed within the diffusion region. These secondary flux ropes are all identified earthward of the observed TCL. These observations further suggest there are numerous small scale structures within the ion diffusion region.

Citation: Wang, R., et al. (2012), Asymmetry in the current sheet and secondary magnetic flux ropes during guide field magnetic reconnection, *J. Geophys. Res.*, *117*, A07223, doi:10.1029/2011JA017384.

¹Space Research Institute, Austrian Academy of Sciences, Graz, Austria.

²Department of Geophysics and Planetary Science, University of Science and Technology of China, Hefei, China.

³Institute of Geology and Geophysics, Chinese Academy of Sciences, Beijing, China.

⁴Swedish Institute of Space Physics, Uppsala, Sweden.

⁵Institute of Space and Astronautical Science, JAXA, Sagami-hara, Japan.

⁶Mullard Space Science Laboratory, Surrey, UK.

⁷State Key Laboratory of Space Weather, Center for Space Science and Applied Research, Chinese Academy of Sciences, Beijing, China.

⁸Center for Space Physics, Boston University, Boston, Massachusetts, USA.

Corresponding author: R. Wang, Space Research Institute, Austrian Academy of Sciences, Graz AT-8042, Austria.
(rongsheng.wang@oeaw.ac.at)

©2012. American Geophysical Union. All Rights Reserved.
10.1029/2011JA017384

1. Introduction

[2] Magnetic reconnection is believed to be the primary candidate for many explosive phenomena in space and laboratory plasmas, during which magnetic energy is efficiently converted by accelerating and heating charged particles and the magnetic field topology changes. In the course of collisionless magnetic reconnection, the ideal frozen-in condition is violated in the diffusion region. In the ion diffusion region, ions are demagnetized while magnetized electrons still move toward the smaller electron diffusion region where electrons are demagnetized also. The decoupling of ions from the magnetized electrons leads to Hall quadrupolar magnetic field and Hall electric field [Sonnerup, 1979; Terasawa, 1983]. This type of quadrupolar magnetic field structure could expand far away from the X-line along the outflow direction [Fujimoto *et al.*, 1997; Nagai *et al.*, 2001, 2003]. In situ spacecraft observations have shown that the energy of the inflow electron beam along the separatrices is very low. The typical energy of the electron beam is about several hundred eV, and the highest energy is less than

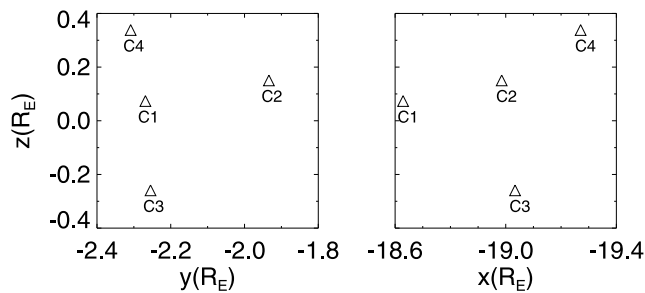


Figure 1a. Cluster tetrahedron location at 10:00 UT on 28 August 2002 in y - z and x - z plane of the GSM coordinates.

5 keV [Nagai et al., 2001, 2003]. The correlated reversals of the ion flows and the reconnected magnetic field as well as Hall electric and magnetic field have been reported by many observational studies [Øieroset et al., 2001; Nagai et al., 2001; Mozer et al., 2002; Nagai et al., 2003; Runov et al., 2003; Deng et al., 2004; Vaivads et al., 2004; Borg et al., 2005; Nakamura et al., 2006; Eastwood et al., 2010a; Wang et al., 2010a]. However, recent simulations indicate that a guide field can dramatically affect the particle dynamics and the structure of the Hall electric field as well as Hall magnetic field in the ion diffusion region [Karimabadi et al., 1999; Pritchett, 2001, 2005; Rogers et al., 2003; Pritchett and Coroniti, 2004; Ricci et al., 2004; Swisdak et al., 2005; Huba, 2005; Fu et al., 2006; Huang et al., 2010], although it does not alter the reconnection rate and the in-plane magnetic field very much [Hesse et al., 2002; Rogers et al., 2003; Pritchett and Coroniti, 2004; Ricci et al., 2004; Huba, 2005; Fu et al., 2006]. Up to now, little attention has been paid to the guide field effect on magnetic reconnection in the spacecraft observational research of the magnetotail. The distorted Hall magnetic field and electric field during a guide field magnetic reconnection has been confirmed by Cluster in the magnetotail [Eastwood et al., 2010b]. In another reconnection event with a weak guide field, the out-of-plane magnetic field still looks like the typical quadrupolar structure if the guide field is removed [Aunai et al., 2011]. An asymmetric current sheet was reported during a magnetic reconnection with a strong guide field [Nakamura et al., 2008], but the spacecraft did not cross throughout the plasma sheet. So, the particle dynamics during guide field reconnection, however, is still poorly understood.

[3] Electron density cavities are another typical characteristic during magnetic reconnection. They lie along the four separatrices in anti-parallel symmetrical reconnection [Shay et al., 2001; Rogers et al., 2003; Lu et al., 2010], whereas in magnetic reconnection with a strong guide field the cavities only appear along one pair of the separatrices and might play an important role in accelerating electrons [Pritchett and Coroniti, 2004; Pritchett, 2005, 2006; Cattell et al., 2005; Drake et al., 2005; Lapenta et al., 2010]. In the magnetotail, the cavity will be created in the northern lobe earthward of the X-line and in the southern lobe tailward of the X-line if the guide field points downward [Pritchett and Coroniti, 2004; Pritchett, 2005, 2006]. The cavities have been confirmed by spacecraft in the magnetotail and at the magnetopause [Øieroset et al., 2001; Mozer et al., 2002;

André et al., 2004; Vaivads et al., 2004; Khotyaintsev et al., 2006; Retinò et al., 2006; Nakamura et al., 2008; Lu et al., 2010]. Previous observations just verified its existence; however, whether the cavity structure will be modified by the guide field hasn't been confirmed by the spacecraft.

[4] Recent near-tail Cluster observation confirmed that magnetic islands/flux ropes could be formed within the center of a single reconnection diffusion region, called secondary magnetic island/flux rope [Wang et al., 2010b, 2010c]. This type of small scale secondary magnetic island has also been observed in the Hall magnetic field region [Eastwood et al., 2007]. The observations confirm the prediction of PIC simulations where magnetic islands could be produced continuously due to the expanded electron current sheet in the equatorial plane of the diffusion region [Karimabadi et al., 2005; Daughton et al., 2006]. Till now, to our knowledge, the observed secondary magnetic islands/flux ropes are all identified in magnetic reconnection without any significant guide field [Eastwood et al., 2007; Wang et al., 2010b, 2010c]. Besides, only a single secondary magnetic island is detected within the ion diffusion region. There is no observational evidence implying that secondary magnetic islands could also be formed in guide field magnetic reconnection.

[5] In this study, a magnetic reconnection event in the presence of a guide field, $\sim 30\%$ of the magnetic field in the plasma sheet boundary layer, is presented. Cluster [Escoubet et al., 2001] crossed the earthward part of the ion diffusion region from the southern hemisphere to the northern hemisphere. This allowed us to study the electromagnetic structure and particle dynamics in detail during this crossing.

2. Observations and Analysis

[6] The spacecraft data used in this paper are obtained from several instruments onboard Cluster. Magnetic field data are taken from the FGM instruments of the four satellites with 4 s and 1/22 s time resolutions [Balogh et al., 2001], ion plasma data from the CIS (CODIF) instruments of C1, C3 and C4 in 4 s resolution [Rème et al., 2001], and electron pitch angle data from the HEEA sensors of the PEACE instruments onboard C1 and C2 in the spin resolution [Johnstone et al., 1997]. The electron pitch angle data are corrected for the spacecraft potential and re-binned in pitch angle using the high-resolution magnetic field data. The spacecraft potential used to deduce the electron density is obtained from the EFW instruments of C1 and C2 [Gustafsson et al., 2001]. Electric and magnetic field wave spectrograms are taken from the STAFF instruments of C1 and C2 [Cornilleau-Wehrin et al., 2003].

[7] During 09:30–11:10 UT on 28 August 2002, Cluster was situated in the magnetotail at $[-19, -2, 0] R_E$ in the GSM coordinates with the separation of about 4000 km. In this interval, a guide field reconnection event has already been identified [Eastwood et al., 2010a]. A large negative IMF B_y (~ -8 nT) was observed for nearly 12 h before the reconnection event (not shown). The relative spacing between all four satellites of Cluster at 10:00 UT are shown in Figure 1a. C4 is located in the northernmost and the separation between C4 and C2 in z direction is $1202 \text{ km} \approx 0.2 R_E \approx 2.9 c/\omega_{pi}$ (R_E is the Earth radius and c/ω_{pi} is ion inertial length, about 416 km for the density

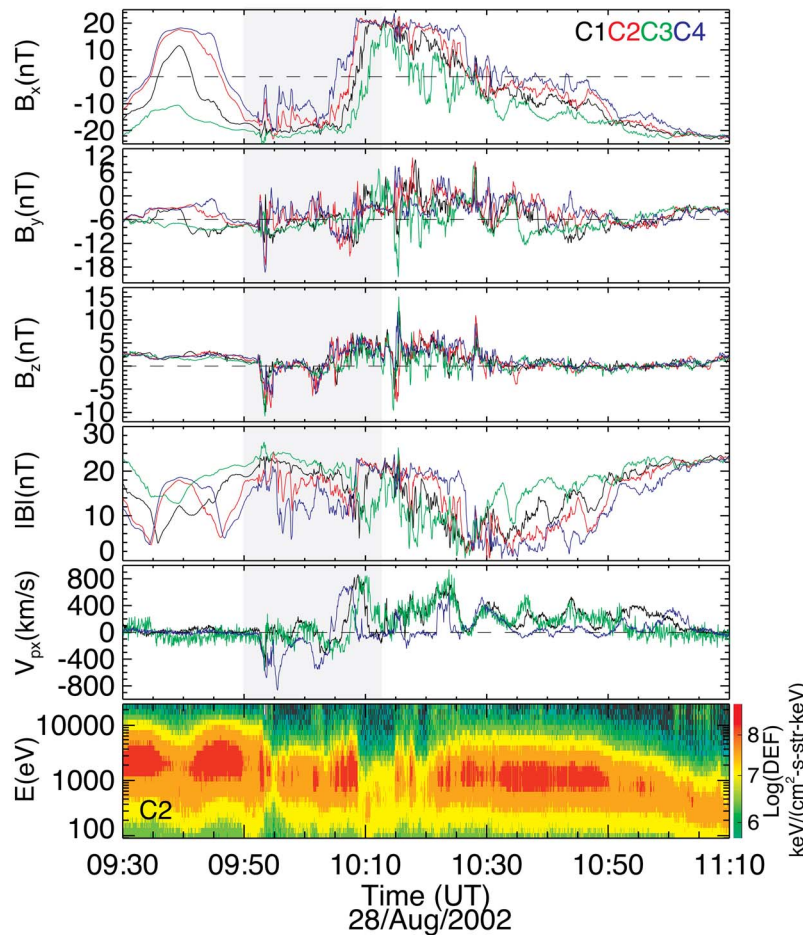


Figure 1b. Cluster observations between 09:30 and 11:10 UT on 28 August 2002 in GSM coordinates are shown. Three components and magnitude of magnetic field with a color scheme of black, red, green and blue for C1 to C4, x component of proton bulk flows v_{px} , and electron energy time spectra from PEACE of C2. The shadow area signifies the time period while Cluster crossed the diffusion region.

0.3 cm^{-3}). C1 is to the south of C2 with a separation distance of $492 \text{ km} \approx 0.08 R_E \approx 1.0 c/\omega_{pi}$. C3 is southernmost and the distance between C3 and C1 in the z direction is $2129 \text{ km} \approx 0.3 R_E \approx 5.0 c/\omega_{pi}$.

2.1. Event Overview

[8] Figure 1b shows magnetic field and plasma data between 09:30 and 11:10 UT with a color scheme of black, red, green, and blue for C1, C2, C2, and C4. From top to bottom, three components and magnitude of magnetic field, x component of proton bulk flow v_{px} , electron energy-time spectra from the PEACE instrument onboard C2 are presented. During the whole interval, Cluster crossed the central current sheet several times. Using the minimum variance analysis (MVA) and Timing method [Russell *et al.*, 1983; Sonnerup and Scheible, 1998; Schwartz, 1998], we find the normal direction of the plasma sheet and minimum variance direction are nearly parallel to the z axis of the GSM coordinates. The maximum variance direction was within 9° of the x direction of the GSM coordinates. So, the GSM coordinates is used through this paper. In the initial interval

between 09:30 and 09:50 UT, C4, C2 and C1 crossed the neutral sheet twice, while C3 was staying in the southern hemisphere. During this interval, plasma bulk flows from the spacecraft were very slow. B_y fluctuated at the four satellites but the average stayed nearly constant -6 nT prior to the onset of high speed flows. This out-of-plane magnetic field called guide field (B_g) is polarity consistent with the IMF B_y . In addition, electron energy spectra in the bottom of Figure 1b imply there was no obvious asymmetric between the northern hemisphere and the southern hemisphere between 09:30 and 09:50 UT. From 09:50 to 10:13 UT (the shadow area in Figure 1b), strong magnetic field oscillation and high speed plasma flows were measured. During this interval, high speed flows up to 800 km/s reversed from tailward to earthward and were accompanied by negative-to-positive reversal of B_z . The observations suggest that Cluster crossed a reconnection site during the interval.

[9] Figure 1c shows $B_y - B_g$ as a function of B_x and V_{px} . The data is taken from C4 between 09:53 and 10:13 UT and from C1 and C3 in the earthward high speed flows (C1 between 1007:31 and 1012:59 UT, and C3 between

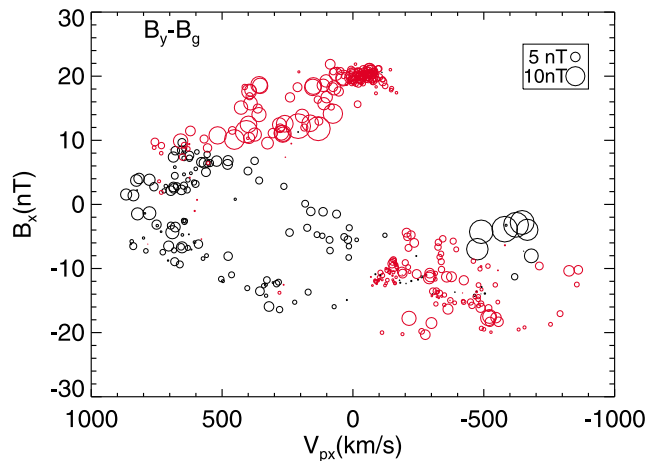


Figure 1c. $B_y - B_g$ as a function of B_x and v_{px} . Black circles correspond to $B_y - B_g < 0$ while red circles denote $B_y - B_g > 0$. The size of the circle corresponds to absolute values of $|B_y - B_g|$. The magnetic field and plasma data from C4 between 0953:14 and 1113:01 UT, from C1 between 1007:31 and 1012:59 UT, and from C3 between 1007:34 and 1012:03 UT are used to make this figure.

1007:34 and 1012:03 UT). Red (black) circles denote $B_y - B_g$ is positive (negative). The size of the circle corresponds to the magnitude of $B_y - B_g$. It is very clear that the out-of-plane magnetic field ($B_y - B_g$) displays an obvious quadrupolar structure. But the quadrupolar structure is distorted. $B_y - B_g$ changes sign at about $|B_x| \approx 9$ nT, unlike in the case of antiparallel reconnection where the Hall magnetic field changes signs at $|B_x| \approx 0$ nT (in the neutral sheet). As we show in the following sections, the distorted quadrupolar structure of the Hall magnetic field could be caused by the addition of the guide field B_g . Based on the correlated reversals of B_z and V_{px} as well as the clear quadrupolar magnetic field, it could be concluded that Cluster passed

through a reconnection diffusion region from tailward to earthward. A schematic illustration is presented in Figure 2. Furthermore, the guide field ($B_g = -6$ nT) is about 30% of the magnetic field in the plasma sheet boundary layer. Note that there is a time delay between B_z and V_{px} reversals, which can be seen more clearly in Figure 3. One possible reason for the delay is presented in the discussion section. It is noticeable that Cluster crossed the diffusion region from the south hemisphere to the north hemisphere in its earthward part between 10:00 and 10:13 UT. In this paper, we mainly concentrate on this crossing.

2.2. Crossing of the Earthward Part of the Ion Diffusion Region

[10] Figure 3 shows electron density (Figure 3a), magnetic field vectors and magnitude (Figures 3b–3e), current density in x and y components obtained from Ampere’s law by magnetic field of C4 and C2 (Figure 3f), electron current density and electron velocity in x component (Figures 3g and 3h), and proton bulk flows in x component during the plasma sheet crossing from 10:00 to 10:13 UT (Figure 3i). The electron density of C1 and C2 is deduced from the spacecraft potential in 0.2 s resolutions and the density of C4 is from the PEACE instrument in 4 s resolution. The deduced electron densities of C1 and C2 are consistent with those from their PEACE instruments and are shown in Figure 3a because of the higher time resolution. Due to the large separation between the satellites, the Curlometer technique could not be used here [Robert *et al.*, 1998]. From the magnetic field, however, all four satellites observed a similar structure of the current sheet. That means the current sheet is nearly stable during the crossing. So, the current density still could be estimated from adjacent two satellites by Ampere’s law: $j_x \approx \frac{\Delta B_y}{\mu \Delta z^2} j_y \approx \frac{\Delta B_x}{\mu \Delta z^2}$. Note that this estimate is still likely to be quantitatively wrong if there is current density structure on scales less than the separation between C2 and C4, but it can be used to examine the qualitative structure of the current density. Using the correlated magnetic field data of C2 and C4, we could derive the current

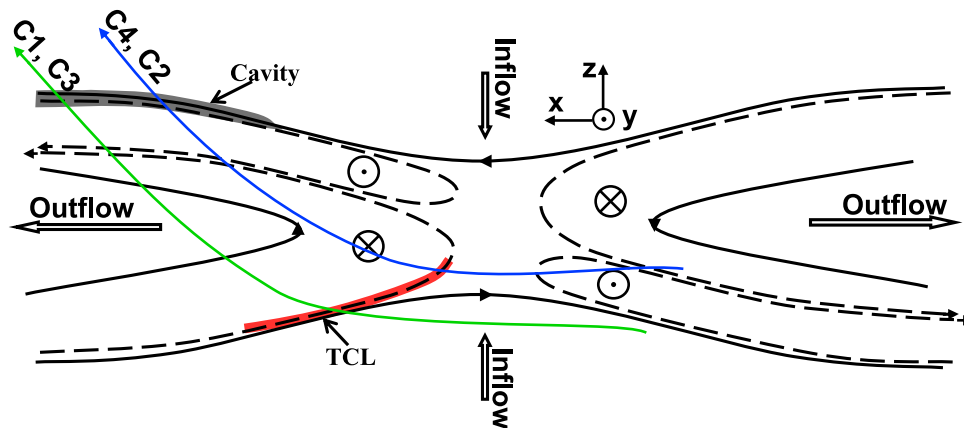


Figure 2. A schematic illustration of the reconnection diffusion region and the trajectory of Cluster crossing it are shown. The black line with arrow denotes magnetic field line. The black dashed line with arrow signifies electron beam. The blue and green lines represent trajectories of C4, C2 and C1, C3. The red thick line denotes the observed thin current sheet (TCL) with the width of ion inertial length. TCL was located along the separatrix which is a line (in 2D projection) separating the reconnecting and reconnected magnetic field. The black area means the density cavity in the separatrix layer.

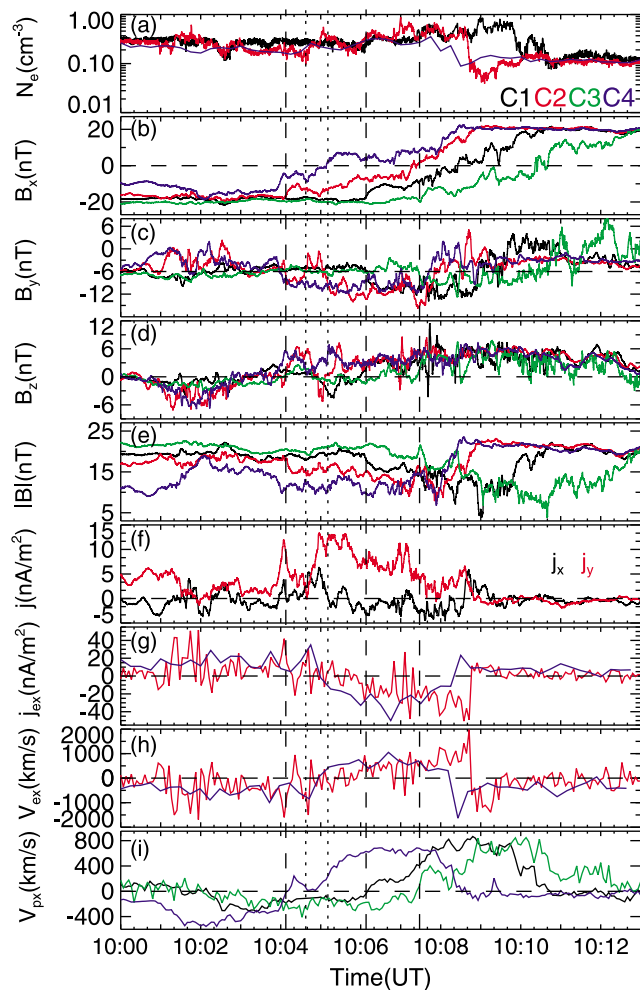


Figure 3. Magnetic field and plasma data during 10:00–10:13 UT are presented. (a) Electron density of C1 and C2 derived from the spacecraft potential and electron density of C4 is obtained from the PEACE instrument. (b–e) Three components and magnitude of magnetic field. (f) The x and y components of current density from Ampere’s law. (g) The x component of electron current density of C4 and C2. (h) The x component electron velocity from C4 and C2. (i) The x component of proton bulk flows from C4, C1 and C3. The three vertical dashed lines correspond to the times when C2, C1, and C3 crossed the southern separatrix layer. The two vertical dotted lines involve a B_z disturbance encountered by C2.

density shown in Figure 3f. Electron current density is calculated as $j_{ex} = en_e v_{ex}$ (only C4 and C2 have electron density and velocity vector data). The three vertical dashed lines in Figure 3 correspond to the times when the spacecraft (C2, C1, and C3) started to enter into the negative Hall quadrant on the earthward side, i.e., the southern separatrix layer. The two vertical dotted lines embrace a B_z disturbance (10:04:38–10:05:12 UT) only encountered by C2.

[11] In the beginning of this interval, all four satellites remained in the southern hemisphere and measured a B_z reversal from negative to positive at about 10:03 UT. One minute later, V_{px} at C4 reversed from tailward to earthward. Nearly simultaneously, the Hall magnetic field B_y – B_g

became negative (the first vertical dashed line). After that, B_x at C4 continued increasing from about -5 nT to 20 nT in the end, accompanied by the reversal of Hall magnetic field B_y – B_g at about 10:07:40 UT when B_x was about 9 nT. So, C4 crossed the diffusion region from tailward to earthward in the southern hemisphere, and then traversed the earthward part of the ion diffusion region from south to north. Finally, C4 was situated in the plasma sheet boundary layer [Lennartsson *et al.*, 2009]. Similar observations were also made by C2 except the B_z disturbance (10:04:38–10:05:12 UT) in the negative Hall quadrant. Moreover, C2 was just below C4 in z direction. So, only one blue curve is used to show the trajectories of C4 and C2 in Figure 2. Starting at $\sim 1006:08$ UT (the second vertical dashed line) for C1 and at about 1007:26 UT (the third dashed line) for C3, they began to measure earthward high speed flows and negative Hall magnetic field B_y – B_g , and then entered into the ion diffusion region, respectively. That is to say, C1 and C3 were in the southern separatrix layer at the times 1006:08 UT and 1007:26 UT, respectively. Afterwards, C1 and C3, remaining south of C2, crossed the earthward ion diffusion region from south to north also. During the crossing (1006:08–10:11 UT for C1 and 1007:26–10:13 UT for C3), they observed a reversal of B_y – B_g from negative to positive as well. In the southern separatrix, both C1 and C3 measured that V_{px} reversed from tailward to earthward. The tailward proton bulk flows were much slower than the earthward flows. In the initial intervals (10:00–1006:08 UT for C1, and 10:00–1007:26 UT for C3), B_x at C1 and C3 remained around -20 nT, B_y – B_g was about -6 nT, and proton bulk flows V_{px} were relatively low. Hence, C1 and C3 were located south of the diffusion region during the initial intervals. The trajectories of C1 and C3 are also schematically shown in Figure 2 (green line). The time sequence of the four satellites entering into the earthward diffusion region is consistent with the relative position order of them in the z direction.

[12] After having entered into the ion diffusion region, all four satellites passed through the central plasma sheet in a time sequence (C4–C2–C1–C3) and finally stayed in the northern plasma sheet boundary layer. Therefore, the velocity of the diffusion region in the z direction can be calculated to be ≈ -7.5 km/s by the timing method [Schwartz, 1998]. C1 and C3 crossed the reconnection site in south of the X-line around 10:03 UT when B_x held nearly constant. Hence, the correlated B_z reversals observed by C1 and C3 enable us to estimate x component velocity of the diffusion region to be -56.5 km/s. Because the velocity of the diffusion region in x direction (V_x) is much larger than that in z direction (V_z), the crossing points in the southern separatrix are much closer to the X-line than the crossing points in the northern separatrix, as indicated in Figure 2. The distance in x direction between the crossing points of the southern separatrix and northern separatrix for each satellite is about 56.5 km/s \times 5 min ~ 41 c/ω_{pi} .

[13] Figure 3a shows electron density from C4, C2 and C1, and there is no data from C3 in this interval. The density fluctuates around 0.3 cm^{-3} from 10:00 to 10:08 UT but there is a sharp dip measured later by C4, C2 and C1 on the northern boundary of the positive Hall magnetic field quadrant, i.e., the northern separatrix. Within the density dip, the magnetic field has a maximum, as shown in Figure 3e.

The density of C2 shows that it drops by $\sim 87\%$ from the level of 0.3 cm^{-3} observed in the diffusion region to 0.04 cm^{-3} inside the dip, and then returned to 0.1 cm^{-3} in the plasma sheet boundary layer. The measurements indicate that the density dip could be the density cavity as mentioned in previous literature [Øieroset et al., 2001; Mozer et al., 2002; André et al., 2004; Vaivads et al., 2004; Khotyaintsev et al., 2006; Retinò et al., 2006]. Within the cavity, there is a weak current directed in the x direction ($j_x > 0$, shown in Figure 3f). The duration of the cavity is about 50 s. Thus, we could obtain its thickness using $V_z \cdot \Delta t_{\text{cavity}} = 7.5 \text{ km/s} \cdot 50 \text{ s} \approx 0.9 c/\omega_{\text{pi}}$. The proton density from CIS also display a density dip in the northern separatrix (not shown here), which further demonstrate the thickness of the cavity should be ion inertial length scale. On the other hand, a thin current layer (TCL) can be identified in the southern separatrix. Figure 3f shows the current density calculated from magnetic field. It is obvious that there is a clear spike of the current density in x and y components at about 10:04 UT when C4 and C2 were located in the southern separatrix. The current density j_x is positive, which means it directs away from the X-line. j_y could reach about 10 nA/m^2 , which is comparable to the current density in the central plasma sheet between 10:06 and 10:07 UT. The duration of the TCL is about 70 s. Then, its thicknesses could be estimated to be $V_z \cdot \Delta t_{\text{TCL}} = 7.5 \text{ km/s} \cdot 70 \text{ s} \approx 1.3 c/\omega_{\text{pi}}$. However, the separation of C4 and C2 in z direction is about $2.9 c/\omega_{\text{pi}}$, which is larger than the thickness of the TCL. So, the current density derived from magnetic field of the two satellites would be underestimated, which could be found more clearly while we compare the current density with electron current density in Figure 3g. Although the current density is underestimated, the profile of the current is evident. We will further discuss it in the following sections. Between the northern and southern boundaries, j_y is totally positive (dawn-dusk direction) and j_x is almost negative except for several very short intervals, e.g., the period when a B_z disturbance is encountered by C2.

[14] Other two satellites C1 and C3 also measured the TCL (gradient in B_x) in the southern separatrix when they crossed it, which will be further analyzed in Figure 5a. C4 and C2 first measured the TCL in the southern separatrix layer at $\sim 10:04\text{UT}$. C3 observed the TCL at last around 10:07:26UT. Then, we can roughly assess the length of the TCL $L_{\text{TCL}} = 56.5 \text{ km/s} \cdot 3 \text{ min } 20 \text{ s} \approx 30 c/\omega_{\text{pi}}$. In the same way, we could get the distance between the cavity observed by C1 and the X-line. The distance is about $56.5 \text{ km/s} \cdot 8 \text{ min} \approx 65 c/\omega_{\text{pi}}$. The result indicates the separatrix layer could extend far away from X-line. According to the observations, it is evident that the density cavity is only observed in the northern separatrix layer while in the southern separatrix layer a thin current layer is measured instead. These observations are different from simulation results [Pritchett and Coroniti, 2004; Pritchett, 2005, 2006] despite the fact that reconnecting magnetic field and the direction of the guide field are consistent with those of the observed reconnection event. In the PIC simulations, the density cavity is only formed in the southern separatrix. In the northern separatrix an electron current layer formed by the outflow electrons is produced [Pritchett and Coroniti, 2004; Pritchett, 2005, 2006].

[15] Electron velocity and electron current density during this crossing are also analyzed. Using the frozen-in condition $\mathbf{E} = -\mathbf{V}_e \times \mathbf{B}$, we checked the reliability of the electron flow velocity. The result indicates the data are basically reliable. More details could be found in the discussion part. Figures 3g and 3h present electron velocity and electron current density $j_{ex} = en_e v_{ex}$ from C4 and C2. The time resolutions of C2 and C4 are 4 s and about 16 s, respectively. There is no data from other two satellites in this interval. From the electron velocity data of C2, electrons move in the negative x direction in the southern (10:04 UT) and northern separatrix (10:09 UT) layers, and v_{ex} can reach about -1500 km/s . While within the Hall region (between the southern and northern separatrices), electrons primarily stream to the positive x direction and electron velocity could get the maximum 2000 km/s around the region where B_y - B_g changes sign from negative to positive. Based on the electron velocity distribution, it could be found clearly that electrons are flowing into the X-line region along the southern and northern separatrix layers while are ejected out from the X-line between two separatrices. The outflow electron has its highest velocity around the B_y - B_g reversal region. Additionally, the maximum velocity of the outflow electrons is larger than that of the inflow electrons. Using the electron velocity, the electron current density could be obtained during this crossing. The electron current density is consistent with the current obtained from magnetic field. In the southern and northern separatrices, the current is directed away from the X-line while it flows into the X-line between the boundaries. The electron current between the northern and southern separatrices is most intense around the B_y - B_g reversal region, and becomes very small within the cavity due to the sudden density dip. The result from C4 is similar to that from C2 even if the data resolution from C4 is so low ($\sim 16 \text{ s}$). In both southern and northern separatrix, the velocity of ion flows is close to 0 km/s . Hence, the current in the separatrix layer is mainly carried by electrons.

[16] Even though the electron current density is more or less consistent with the current density from magnetic field, the magnitude of the electron current density is stronger, as shown in Figures 3f and 3g. For example, in the southern separatrix, the electron current density is about 30 nA/m^2 while the current from magnetic field is less than 5 nA/m^2 in x component. Such difference might be caused due to the large separation between C4 and C2, as mentioned above. $\Delta Z_{C4, C2}$ is about $2.9 c/\omega_{\text{pi}}$, which is larger than the thickness of the thin current layer $1.3 c/\omega_{\text{pi}}$. Hence, the current density from magnetic field is underestimated. In first panel of Figure 5a, the current density calculated from Ampere's law by magnetic field of C2 and C1 is shown as well. The separation between C2 and C1 in z component is about $1.0 c/\omega_{\text{pi}}$ smaller than that of C4 and C2. Thus, the current density became more intense ($\sim 20 \text{ nA/m}^2$) than that from C4 and C1. This enhancement of current density from C2 and C1 further indicates the current density from C4 and C2 is underestimated due to the large separation. Although the current density is underestimated, the TCL in the southern separatrix is still apparent.

[17] Electron density (Figure 4a), x and y components of magnetic field (Figures 4b and 4c), high energy electron omni-directional energy fluxes ($>35 \text{ keV}$) (Figures 4d and 4e), low to medium electron energy time spectra

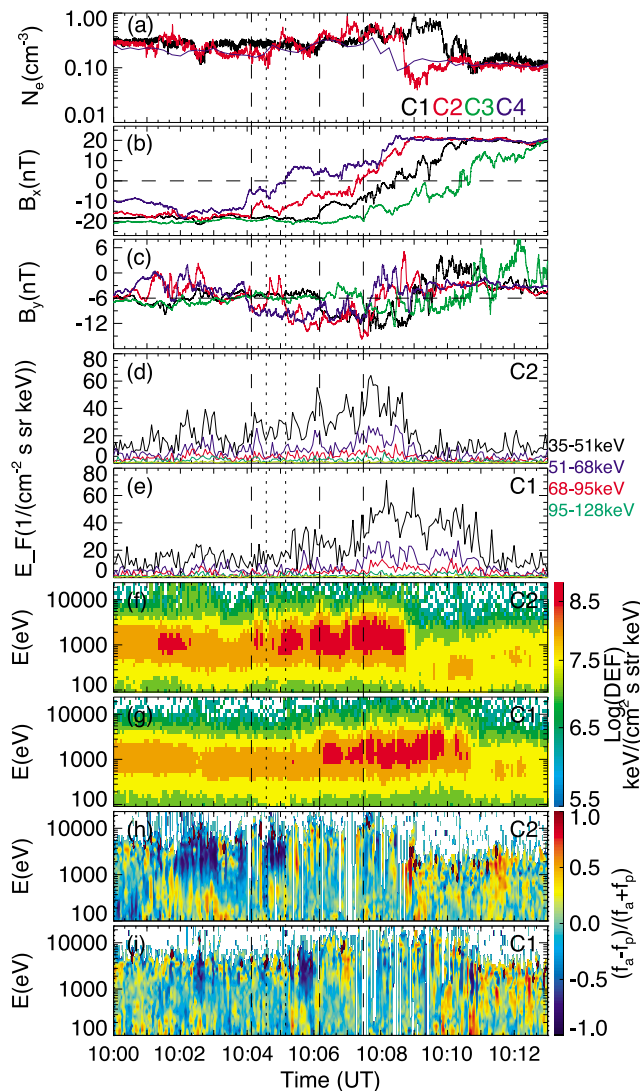


Figure 4. Electron energy spectra, field-aligned anisotropic distribution and energetic electron fluxes are shown in the same time interval as in Figure 3. The five vertical lines correspond to the same times as in Figure 3 also. Electron density, x and y components of magnetic field, energetic electron fluxes (>35 keV) from C2 and C1, electron energy spectra and electron field-aligned anisotropic distribution $(f_a - f_p)/(f_a + f_p)$ from C2 and C1 are shown from top to bottom. Here f_a and f_p are the phase space density antiparallel and parallel to magnetic field, respectively.

(Figures 4f and 4g), and electron field-aligned anisotropic distribution (100 eV \sim 23 keV) from C1 and C2 (Figures 4h and 4i) are shown in Figure 4. The five vertical lines correspond to the same times labeled in Figure 3. The electron field-aligned anisotropic distribution is defined as $(f_a - f_p)/(f_a + f_p)$, where f_a and f_p are phase space density antiparallel and parallel to the magnetic field respectively. Gaps in Figures 4h and 4i denote no data in the parallel and/or antiparallel directions. Since the electron distributions from C4 (C3) are very similar to those from C2 (C1). Only the electron distributions from C1 and C2 are shown. During the earthward crossing of the ion diffusion region, the phase

space density in parallel and antiparallel directions is larger than that in the perpendicular direction, which could be seen in Figure 6. So, we only show field-aligned anisotropic distribution in Figure 4. From Figure 4h, electrons from 800 eV to 10 keV at C2 are flowing parallel to the magnetic field (blue) around the TCL (1003:40 \sim 10:04 UT). While within the density cavity, electrons are moving antiparallel to magnetic field (red, \sim 10:09 UT). So, electrons are injected into the X-line along the southern (the TCL) and northern (the cavity) separatrix layers. Between the TCL and the cavity excluding the B_z disturbance labeled by two vertical dotted lines, the electron field-aligned anisotropic distribution in energies from 1 keV to 10 keV is still clear. In the southern hemisphere (1004:20–1007:20 UT) excluding the disturbance, many spiky red regions (above 1 keV) could be found. While in the northern hemisphere (1007:20–1008:40 UT), several clear blue regions (above 1 keV) are found. These observations indicate electrons are mainly flowing out from the X-line between the northern and southern separatrix layers. The energy of the outflow electrons could reach 20 keV around the B_y - B_z reversal region. The highest energy of the inflow electron could extend up to 10 keV in the TCL and cavity. In the plasma sheet boundary layer, electrons also display field-aligned anisotropy but the energy of the electrons becomes lower. A similar electron distribution was measured by C1. In Figures 4d and 4e, fluxes of energetic electrons (>35 keV) are enhanced around the center of the plasma sheet. The fluxes are very high also in the B_y - B_z reverse region. In the TCL (around the first vertical dashed line for C2 and the second dashed line for C1), the level of the fluxes becomes lower but there is a clear peak there. The fluxes gradually decreased as the spacecraft approached the cavity and became very low within the cavity.

[18] Figure 5a shows the current density (j_{\parallel}, j_{\perp}) estimated from Ampere's law using the magnetic field data of C2 and C1, two components of electric field (E_x, E_y) in the spacecraft Inverted Spin Reference (ISR2) coordinates, fluxes of energetic electrons, electron field-aligned anisotropic distribution, electron energy spectra, and wave spectrogram of magnetic field as well as electric field from C1 around the TCL. Except for the first panel presenting the electron density, Figure 5b shows the data from C2 inside the cavity in the same format as Figure 5a. From the first panel of Figure 5a, the TCL primarily consisted of the current antiparallel to magnetic field. At the same time, a strong electron inflow from 600 eV to 10 keV parallel to magnetic field is measured (blue area). Hence, the observed TCL is formed by the inflow electron. The energy of the inflow electron reaches up to 10 keV which is the upper energy limit of the PEACE instrument at that time. Furthermore, energetic electron fluxes in the energy channels of 37–95 keV have an obvious peak within the TCL. On the other hand, an inflowing electron antiparallel to the magnetic field is measured in the cavity (red area), as shown in the fourth panel of Figure 5b. The energy of the electron can extend up to 7 keV. The fluxes of energetic electrons are low within the cavity, yet there is a slight increase within the cavity for the first two energy channels, especially for the second energy channel (51–68 keV). According to the observations, electrons could be accelerated while stream into the X-line along the southern and northern separatrix layers. The energy of

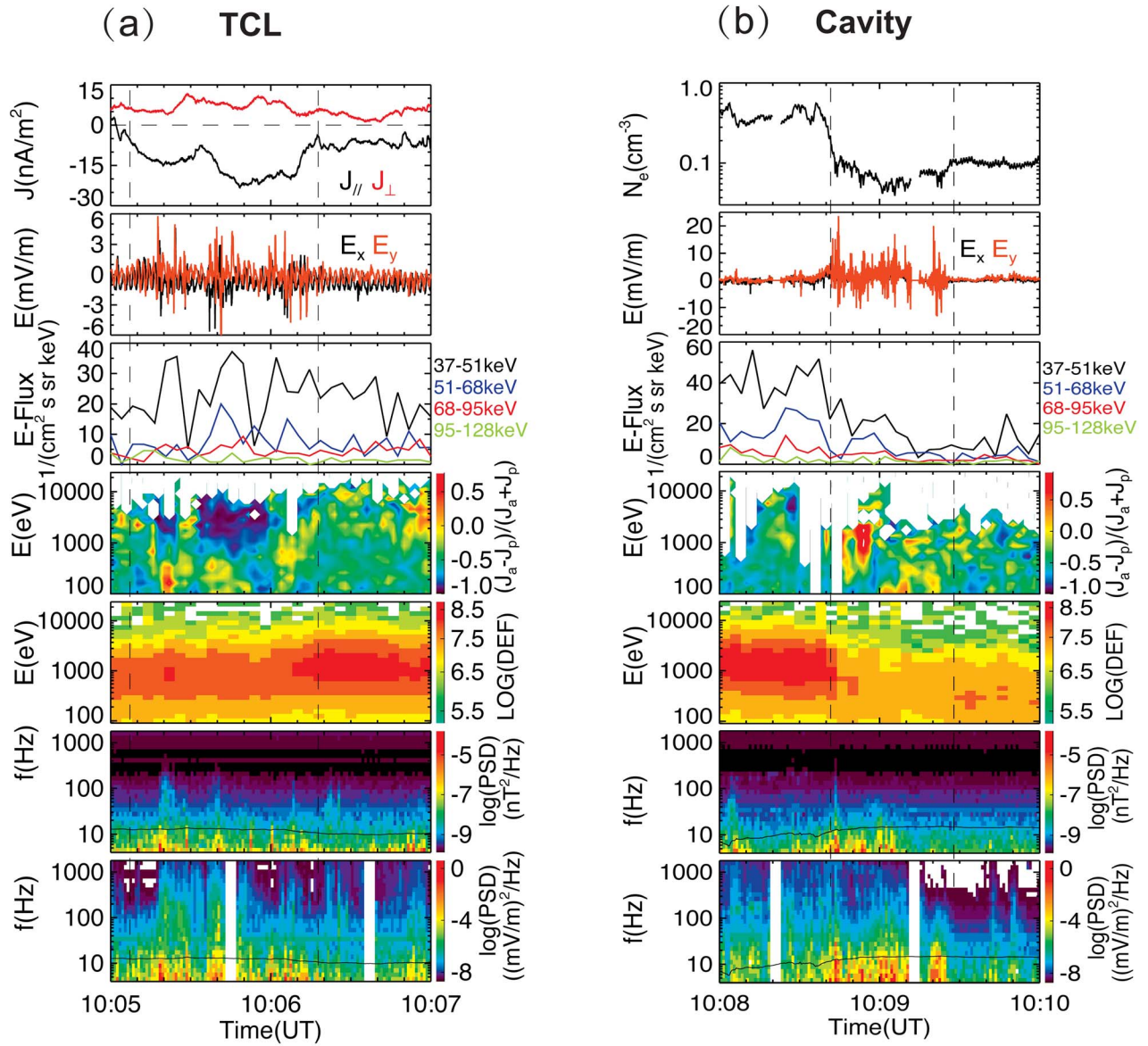


Figure 5. (a) J_{\parallel} and J_{\perp} components of current density estimated from Ampere's law by magnetic field data of C1 and C2, two components (E_x , E_y) of electric field in ISR2 coordinates, energetic electron fluxes, electron field-aligned anisotropic distribution, electron energy spectra, wave spectrogram of magnetic field and electric field from C1 around the thin current sheet (TCL) in the southern separatrix layer are shown. (b) Electron density, two components of electric field, energetic electron fluxes, electron field-aligned anisotropic distribution, electron energy spectra, and wave spectrogram of magnetic field and electric field from C2 around the density cavity in the northern separatrix layer is presented. The curves in the last two panels denote the lower hybrid wave frequencies.

the inflow electron could reach 10 keV. The energy of the inflow electrons might extend to higher energies based on the energetic electron fluxes in both regions. In both the TCL and the cavity, electric field becomes stronger. The maximum of the electric field within the cavity can reach 20 mV/m. The waves below the lower hybrid frequencies (black curves in the bottom two panels of Figures 5a and 5b) are intensified also. In addition, the electron energy spectra (the fifth panels in Figure 5) also show the electron energy fluxes become intense in the TCL while weak in the cavity.

According to these observations, it seems that more energetic electrons are observed in the TCL than in the cavity.

[19] Figure 6 shows several typical electron pitch angle distributions in three regions the TCL (Figure 6a), B_y - B_g reversal region (Figure 6b), and the cavity (Figure 6c). The black, dashed, and red lines correspond to the phase space density (PSD) in parallel, perpendicular and antiparallel to magnetic field. The dotted line is the one count level. In the TCL, the PSD parallel to magnetic field is larger than other two directions at energies larger than 1 keV. In the cavity,

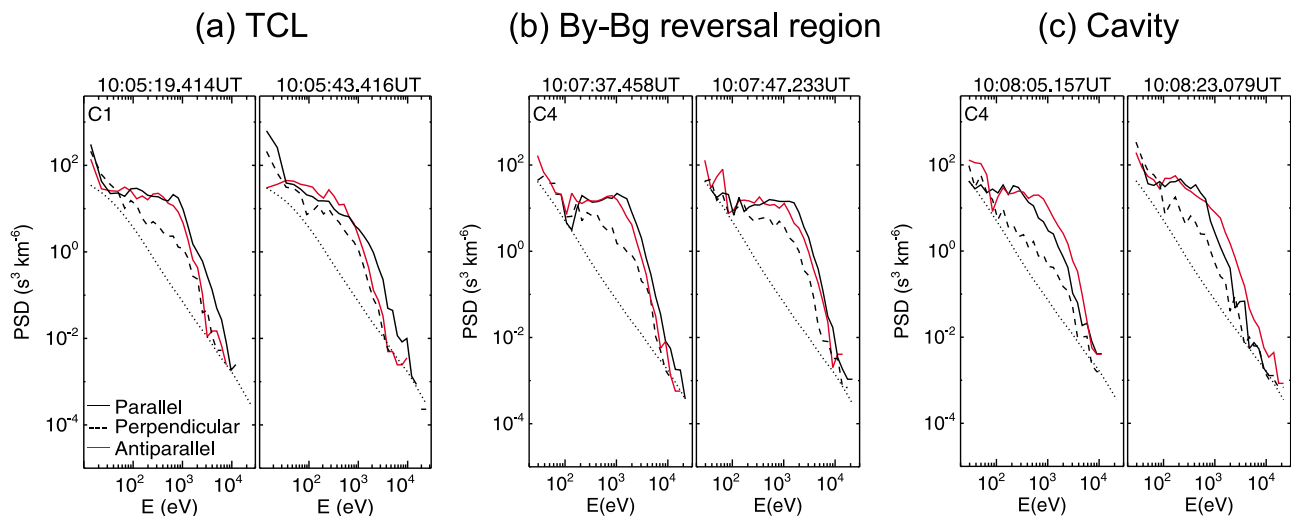


Figure 6. Electron pitch angle distribution in three regions: (a) the thin current sheet (TCL) in the southern separatrix layer, (b) outflow electron region (around the region where B_y - B_g changes sign from negative to positive) and (c) the density cavity. The black, dashed, and red lines correspond to the phase space density in parallel, perpendicular and antiparallel to magnetic field. The dotted line is the one count level.

the PSD antiparallel to magnetic field is higher than other directions at energies larger than 800 eV. This distribution indicates electrons are injected into the X-line in these regions. The energy of the inflow electron can exceed 10 keV sometimes. In the B_y - B_g reversal region, the PSD (>1 keV) in the parallel direction is higher than in the perpendicular and antiparallel directions. So, electrons are flowing out from the X-line along the magnetic field. Electrons display a flat-top distribution between the northern and southern separatrices. The shoulder energy is about between 100 eV to 2 keV. This distributional feature could be seen in Figure 6b. The non-isotropic electron outflow has also been observed recently in other reconnection events [Borg *et al.*, 2012; Wang *et al.*, 2010a].

2.3. Multiple Secondary Magnetic Flux Ropes

[20] Figure 7 represents magnetic field and electron density in the interval 10:06–10:09UT when the four satellites were located within the plasma sheet. In this interval, three evident bipolar signatures of B_z with sign changes are measured separately, as labeled by three vertical dotted lines in the figure. In the first and third bipolar B_z , electron density has a clear peak. For the second bipolar B_z , although no obvious electron density peak, the density was enhanced around the bipolar B_z also. In the first two bipolar B_z signatures, the out-of-plane magnetic field (core magnetic field B_y) was very strong. Especially, there was a clear peak of B_y in the second bipolar B_z . In the third bipolar B_z signature, $|B_y|$ became very weak, only about 6 nT. Nevertheless, there was a core magnetic field within all three bipolar B_z signatures. Thus, the three bipolar B_z correspond to three magnetic flux ropes within the ion diffusion region, called secondary magnetic flux ropes [Wang *et al.*, 2010b, 2010c]. The B_z perturbation changes sign from negative to positive, which indicates all the flux ropes are moving earthward. Three secondary magnetic flux ropes are all measured in the southern hemisphere ($B_x < 0$) after the spacecraft passed through the TCL, while in the northern hemisphere, no

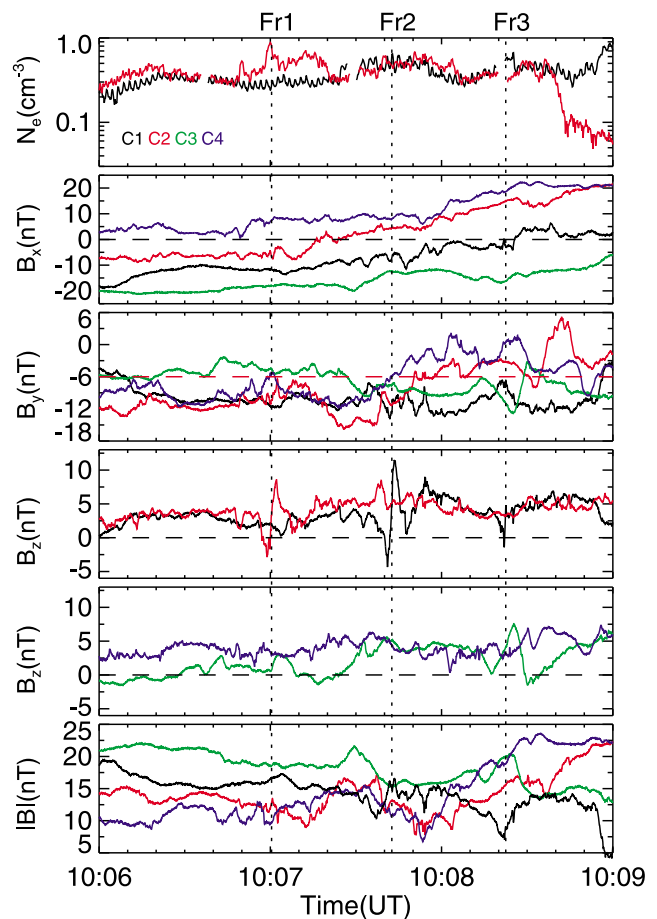


Figure 7. Electron density and magnetic field data are shown. The three vertical dotted lines correspond to three bipolar B_z (Fr1, Fr2 and Fr3) with sign change.

significant bipolar B_z involving sign change are detected, even though the spacecraft also stayed there for a long time. The durations for the secondary magnetic flux ropes (Fr1, Fr2 and Fr3) are only 7 s, 10 s and 3 s, respectively. The distance between C4 and C2 in z direction is about $2 c/\omega_{pi}$. C4 is located tailward of C2. However, no substantial bipolar B_z was observed by C4 before C2 measured the first island. So, the island size is about ion inertial length scale at most. The temporal spacing between any two adjacent flux ropes was about $40 \text{ s} \approx 8 T_i$ (T_i proton cyclotron period).

3. Discussion

[21] The satellites C4, C1 and C3 detected reversals of x component of proton bulk flows v_{px} in the southern separatrix in turn. Whereas they observed reversals of B_z almost at the same time (about 10:03 UT). Besides, there is a time delay between the reversals of v_{px} and B_z for each satellite. The time span between reversals of B_z and V_{px} are nearly 1, 3, and 4 min for C4, C1, and C3, respectively. In other words, the farther the spacecraft leaves away from the neutral sheet in the southern hemisphere, the longer the time span between B_z and V_{px} is. One possible reason for the time delay is the presence of the guide field. In antiparallel magnetic reconnection, the reconnected magnetic field and accelerated ion are jetting symmetrically from the X-line along the $\pm x$ axis. So, the coincident reversals of v_{px} and B_z will be observed as long as the spacecraft crosses the diffusion region along the x axis. However, ion dynamics is severely changed in guide field reconnection from numerical simulations [Karimabadi et al., 1999; Pritchett, 2001, 2006; Rogers et al., 2003; Pritchett and Coroniti, 2004; Ricci et al., 2004; Huba, 2005; Huang et al., 2010]. In the simulations where the reconnecting magnetic field and the direction of the guide field is consistent with our reconnection event in the tail, ions flow earthward above the lower left and upper right separatrices while ions stream tailward below the pair of the separatrices [Pritchett and Coroniti, 2004, Figure 9a]. Although the ion flows are deflected, the in-plane magnetic field isn't alerted [Pritchett and Coroniti, 2004; Hesse et al., 2002]. As a result, the spacecraft will measure v_{px} reversals in the separatrix and a time delay of the reversals between v_{px} and B_z , as it crosses the diffusion region along the x direction. The mechanism for the deflection of ion flows in guide field reconnection remains an issue. One explanation is that the E_z component resulting from the charging of separatrices cause the ion flow deflection [Pritchett and Coroniti, 2004].

[22] Asymmetrical structure of the Hall quadrupolar magnetic field is investigated during this guide field reconnection. The quadrupolar structure is still clear but distorted to the northern hemisphere in the earthward part while to the southern hemisphere in the tailward. The Hall current system is examined in detail also by the current density estimated from electron moments and magnetic field. In the northern and southern separatrix layers, electrons flowing into the X-line are measured. While, between the northern and southern separatrices, electrons are mainly flowing out from the X-line. The outflow electrons are most evident around the B_y - B_g reversal region, where the current density resulting from the outflow electrons has the maximum. In other words, the outflow electron current is deflected to the northern

hemisphere. It contrasts to the case in antiparallel reconnection where the accelerated electrons are jetting along the $\pm x$ axis [Karimabadi et al., 2007; Phan et al., 2007; Shay et al., 2007]. This type of electron velocity distribution creates the distorted Hall electron current system and then the observed quadrupolar structure. The current estimated from magnetic field further verified the Hall electron current system. The distortion of the quadrupolar structure has also been observed in the linear theory of tearing mode [Daughton and Karimabadi, 2005]. Another mechanism for the generation of the quadrupolar structure is ion kinetics as predicted by Karimabadi et al. [2004].

[23] Since the presence of the guide field, the outflow electron current layer in the earthward part of the reconnection diffusion region is exerted by the Lorentz force $f_z = j_{ex} \times B_g (j_{ex} < 0, B_g < 0, f_z > 0)$ in the vicinity of X line. The force directs to the north and positively relates with the intensity of the guide field. Hence, the outflow electron current layer is deflected to the northern hemisphere, while the guide field is moderate. As a result, the distortion of the quadrupolar structure will be generated. The observations are consistent with the recent simulation results where a very weak guide field could strongly deflect the out jets [Goldman et al., 2011], and also consistent with the picture derived by Eastwood et al. [2010b] in analyzing another guide field reconnection event.

[24] Electron acceleration mechanism is another controversial issue in magnetic reconnection research. The observations have demonstrated a fair amount of magnetic energy could be converted into energetic electrons over the energy range from a few ten keV to a few hundred keV [Øieroset et al., 2002; Imada et al., 2007; Åsnes et al., 2008; Wang et al., 2010]. Electrons experience two-step acceleration during magnetic reconnection [Hoshino et al., 2001; Imada et al., 2007; Wang et al., 2008]. They are accelerated first in the electron diffusion region and then further accelerated in the pile-up regions [Hoshino et al., 2001; Øieroset et al., 2002; Imada et al., 2007; Wang et al., 2008]. In our event, however, an energetic electron inflow up to 10 keV is measured in both northern and southern separatrix layers. The fluxes of energetic electrons up to 95 keV have a clear peak in the southern separatrix layers (the TCL). The fluxes up to 51 keV have a slight increase in the northern hemisphere (the cavity) also. These observations indicate the energy of the inflow electrons might extend to higher energy. According to the measurement, electrons could be pre-accelerated along the separatrix before they enter into the electron diffusion region. Electron acceleration in the separatrix layer has been proposed in several PIC simulations [Pritchett, 2001; Pritchett and Coroniti, 2004; Cattell et al., 2005; Drake et al., 2005; Huang et al., 2010; Lapenta et al., 2010]. Parallel electric field [Pritchett, 2001; Pritchett and Coroniti, 2004;], electron holes [Drake et al., 2003; Matsumoto et al., 2003; Cattell et al., 2005; Andersson et al., 2009; Lapenta et al., 2011], and different kinds of waves (e.g., lower hybrid waves) are all probably contribute to electron acceleration in the region. As more and more electrons are accelerated and injected into the X-line region along the separatrix layer, a density cavity would be formed in the outer end of the separatrix layers. Afterwards, this cavity will elongate toward the X-line along the separatrix layer as magnetic reconnection

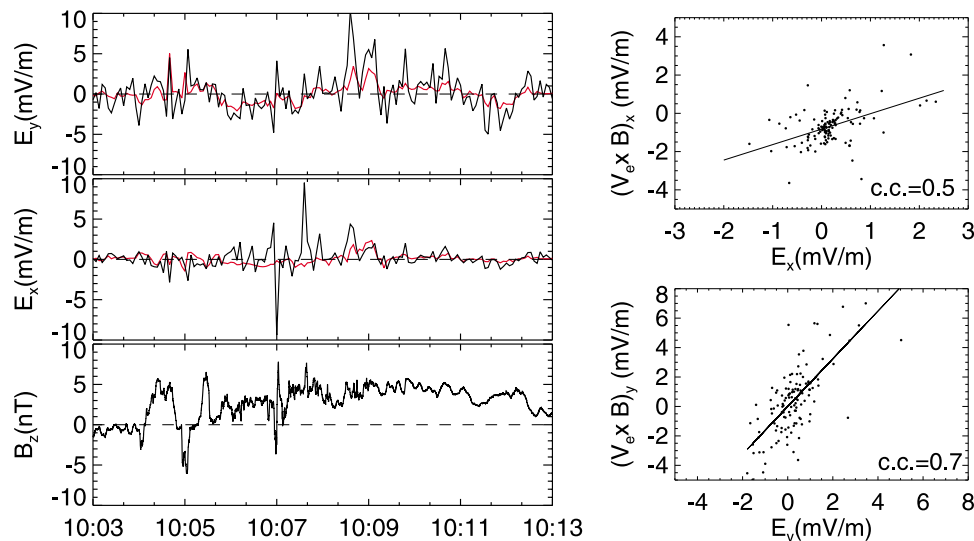


Figure 8. (left) Electric field components E_x (red) and $(\mathbf{V}_e \times \mathbf{B})_x$ (black), E_y (red) and $(\mathbf{V}_e \times \mathbf{B})_y$ (black), and magnetic field component B_z from the spacecraft C2. The electric field data are shown in ISR coordinates and the magnetic field data are shown in GSM coordinates. (right) Scatterplots of electric field components E_x versus $(\mathbf{V}_e \times \mathbf{B})_x$ and E_y versus $(\mathbf{V}_e \times \mathbf{B})_y$ between 10:03 and 10:13 UT excluding the interval 1006:30 and 1008:10 UT when several spikes of $(\mathbf{V}_e \times \mathbf{B})_x$ were observed. The correlation coefficients are displayed in the bottom.

continues. So, if the spacecraft crossed the northern and southern separatrix layers in a tilted trajectory as the orbit of the spacecraft in Figure 2, the cavity might be just measured in one separatrix while in the other separatrix an electron current layer is observed. This gives us a reasonable explanation why the cavity is only measured in the northern separatrix layer while a TCL is encountered in the southern separatrix layer in our event.

[25] Our observations verify the inflow electron thin current layer (TCL) in the southern separatrix and the density cavity in the northern separatrix. A possible reason for the absence of the density cavity in the southern separatrix is that the density cavity in the southern separatrix hadn't extended to the locations where the spacecraft passed by. The measurement is dramatically different from the simulation result [Pritchett and Coroniti, 2004; Pritchett, 2005, 2006] where electron density cavity is created in the southern separatrix while a thin electron current layer is formed by outflow electrons in the northern separatrix. The contradiction between the observation and simulation might be caused by the different intensity of the guide field. In the simulations, ratio between the guide field B_g and the asymptotic reconnecting field B_0 is about 1. However, the ratio is only about 0.3 in our event. Since the outflow electron layer in the earthward part of the reconnection diffusion region is exerted by the Lorentz force $f_z = j_{ex} \times B_g (j_{ex} < 0, B_g < 0, f_z > 0)$, if the force is strong enough due to the intense guide field, the outflow electron layer will overlap with the northern separatrix. As a result, the outflow electron current layer in the northern separatrix will be formed, as predicted in the simulations [Pritchett and Coroniti, 2004; Pritchett, 2005, 2006].

[26] The simulations and observations indicate there is a strong electric field perpendicular to local magnetic field along the separatrix layer [Pritchett, 2005; Mozer et al.,

2002]. This perpendicular electric field will drain ions in the separatrix layer away. Because of the decrease of ions, electrons will also escape the regions rapidly along the magnetic field to maintain the electric neutrality. So, a density cavity along the separatrix layer will be created. This is another possible mechanism for the formation of the cavity. In this event, the electric field is really enhanced within the separatrix layers. However, we cannot determine whether the enhancement of the electric field is from the parallel component or perpendicular components because only two components of electric field are measured by Cluster.

[27] Multiple secondary magnetic flux ropes within the ion diffusion region are reported here. They are all moving earthward and were encountered earthward of the TCL. Besides, they are measured in the southern hemisphere. In the northern hemisphere where the outflow electron current layer is observed, however, no magnetic flux ropes are measured even though the spacecraft stayed there for a long time also. The reason is still unclear. Recently, numerical simulations suggest the thin current layer formed by the outflow electrons along the separatrix is unstable to secondary flux ropes [Karimabadi et al., 2005; Daughton et al., 2011; Huang et al., 2011]. In the simulations, the thin current layer is electron scale and numerous secondary magnetic flux ropes could be formed in the thin current sheet along the separatrix [Daughton et al., 2011]. Although our observations possibly resemble the simulations, our observations are ion scale. On the origin of the observed flux ropes in our event, another paper is being prepared to discuss it. Anyway, the observations further confirm that the gross X-line picture for magnetic reconnection is only an average sense, as proposed by Nakamura et al. [2006].

[28] Figure 8 shows electric field components $E_{x,y}$ (red) from the EFW instrument and $(\mathbf{V}_e \times \mathbf{B})_{x,y}$ (black), and magnetic field component B_z from the spacecraft C2 in the

left. In the right, we show scatterplots of electric field components E_x versus $(\mathbf{V}_e \times \mathbf{B})_x$, and E_y versus $(\mathbf{V}_e \times \mathbf{B})_y$ between 10:03 and 10:13 UT excluding the interval 1006:30 and 1008:10 UT when several spikes of $(\mathbf{V}_e \times \mathbf{B})_x$ were observed. The correlation coefficients are displayed in the bottom. It can be seen that the spike of $(\mathbf{V}_e \times \mathbf{B})_x$ at about 10:07 UT corresponds to the flux rope Fr1. While the spike of $(\mathbf{V}_e \times \mathbf{B})_x$ at about 1007:40 UT corresponds to a further enhancement of B_z associated with the flux rope Fr2. Excluding this short interval, it is clear that E_y and $(\mathbf{V}_e \times \mathbf{B})_y$ are significant correlated (The correlation coefficient c.c. = 0.7). So, the electron flow velocity in x component which we used in this paper is basically reliable. The correlation coefficient between E_x and $(\mathbf{V}_e \times \mathbf{B})_x$ is about 0.5. In this interval, E_x from the EFW instrument was very weak. The average value was about 0.2 mV/m which was comparable to the offset. That should be the reason for the low c.c. The large deviation between E_x and $(\mathbf{V}_e \times \mathbf{B})_x$ around and within the flux ropes is very apparent. Around the flux ropes, electron fluxes are obviously enhanced (not shown here). It seems electrons could be accelerated around the flux ropes. So, the electric field within the flux ropes should be more complicated than the 4 s average data. The high resolution data indeed support this point (not shown). More details about the flux ropes and associated enhancement B_z could be found in another paper as mentioned above. On the other hand, the flux ropes moved earthward with a velocity of about 400 km/s which is several tens of times than the velocity of the plasma sheet in z direction (-7.5 km/s). Electron temperature gradient around the flux ropes is strong. There are at most two data points within the flux ropes. In other words, the electron moment calculation around the flux ropes might be affected by time aliasing due to such quick motion of magnetic flux ropes.

4. Conclusions

[29] Using the Cluster observations in the near-Earth magnetotail, we explored a magnetic reconnection event with a moderate guide field, about 30% of the magnetic field in plasma sheet boundary. Cluster passed through the magnetic reconnection site from tailward to earthward, and then crossed the earthward part of the ion diffusion region from south to north. The crossing of the earthward diffusion region is studied in detail and several main conclusions are presented as follows.

[30] 1. During the crossing of the ion diffusion region earthward of the X-line, electrons flowing into the X-line are observed along both the northern and southern separatrix layers. These inflow electrons form the electron current directing away from the X-line. Between both separatrices, electrons are mainly jetting out from the X-line. The electron current density gets its maximum at the $B_y - B_g$ reversal region. This kind of electron current system produces the observed distorted quadrupolar structure of Hall magnetic field.

[31] 2. In the northern separatrix layer, an electron density cavity is detected, while in the southern separatrix, instead of a density cavity, a thin current layer is identified. The current is streaming out from the X-line and is formed due to the inflow electron. The thickness of the TCL and the cavity is about the ion inertial length. The length of the TCL can

achieve $30 c/\omega_{pi}$. This asymmetry between the northern and southern separatrix layers is reported for the first time.

[32] 3. In the northern and southern separatrix layer, inflowing electrons up to 10 keV are detected. Energetic electron (up to 90 keV) fluxes have an evident increase in the separatrix layer. That means the energy of the inflow electrons might extend to higher energy. So, electrons could be pre-accelerated along the separatrices before they are ejected into the electron diffusion region. More energetic electrons are observed in the TCL than in the cavity.

[33] 4. Multiple secondary magnetic flux ropes are observed inside the ion diffusion region. All the secondary magnetic flux ropes were moving earthward and were detected in the earthward of the observed TCL.

[34] **Acknowledgments.** The authors thank Steven J. Schwartz, Andris Vaivads and H. Hasegawa for helpful discussion and comments. Cluster data are obtained from the ESA Cluster Active Archive. We thank the FGM, CIS, PEACE, RAPID, EFW, and STAFF instrument teams and the ESA Cluster Active Archive. This work is partly supported by the Austrian Science Fund (FWF) I429-N16. This work in China is supported by the National Science Foundation of China (NSFC) grants (41174122 and 41104092) and China Postdoctoral Science Foundation Funded Project (2011M500030).

[35] Philippa Browning thanks the reviewers for their assistance in evaluating the paper.

References

- Andersson, L., et al. (2009), New features of electron phase space holes observed by the THEMIS mission, *Phys. Rev. Lett.*, *102*(22), 225004 doi:10.1103/PhysRevLett.102.225004.
- André, M., A. Vaivads, S. C. Buchert, A. N. Fazakerley, and A. Lahiff (2004), Thin electron-scale layers at the magnetopause, *Geophys. Res. Lett.*, *31*, L03803, doi:10.1029/2003GL018137.
- Åsnes, A., M. G. G. T. Taylor, A. L. Borg, B. Lavraud, R. W. H. Friedel, C. P. Escoubet, H. Laakso, P. Daly, and A. N. Fazakerley (2008), Multispacecraft observation of electron beam in reconnection region, *J. Geophys. Res.*, *113*, A07S30, doi:10.1029/2007JA012770.
- Aunai, N., A. Retino, G. Belmont, R. Smets, B. Lavraud, and A. Vaivads (2011), The proton pressure tensor as a new proxy of the proton decoupling region in collisionless magnetic reconnection, *Ann. Geophys.*, *29*, 1571–1579, doi:10.5194/angeo-29-1571-2011.
- Balogh, A., et al. (2001), The Cluster Magnetic Field Investigation: Overview of in-flight performance and initial results, *Ann. Geophys.*, *19*(10-12), 1207–1217, doi:10.5194/angeo-19-1207-2001.
- Borg, A. L., M. Øieroset, T. D. Phan, F. S. Mozer, A. Pedersen, C. Moukik, J. P. McFadden, C. Twitty, A. Balogh, and H. Rème (2005), Cluster encounter of a magnetic reconnection diffusion region in the near-Earth magnetotail on September 19, 2003, *Geophys. Res. Lett.*, *32*, L19105, doi:10.1029/2005GL023794.
- Borg, A. L., M. G. G. T. Taylor, and J. P. Eastwood (2012), Electron pitch angle distribution during magnetic reconnection diffusion region observations in the Earth's magnetotail, *Ann. Geophys.*, *30*, 109–117, doi:10.5194/angeo-30-109-2012.
- Cattell, C., et al. (2005), Cluster observations of electron holes in association with magnetotail reconnection and comparison to simulations, *J. Geophys. Res.*, *110*, A01211, doi:10.1029/2004JA010519.
- Cornilleau-Wehrin, N., et al. (2003), First results obtained by the Cluster STAFF experiment, *Ann. Geophys.*, *21*(2), 437–456, doi:10.5194/angeo-21-437-2003.
- Daughton, W., and H. Karimabadi (2005), Kinetic theory of collisionless tearing at the magnetopause, *J. Geophys. Res.*, *110*, A03217, doi:10.1029/2004JA010751.
- Daughton, W., J. Scudder, and H. Karimabadi (2006), Fully kinetic simulations of undriven magnetic reconnection with open boundary conditions, *Phys. Plasmas*, *13*(7), 072101, doi:10.1063/1.2218817.
- Daughton, W., V. Roytershteyn, H. Karimabadi, L. Yin, B. J. Albright, B. Bergen, and K. J. Bowers (2011), Role of electron physics in the development of turbulent magnetic reconnection in collisionless plasmas, *Nat. Phys.*, *7*(7), 539–542, doi:10.1038/nphys1965.
- Deng, X. H., H. Matsumoto, H. Kojima, T. Mukai, R. R. Anderson, W. Baumjohann, and R. Nakamura (2004), Geotail encounter with reconnection diffusion region in the Earth's magnetotail: Evidence of multiple

- X lines collisionless reconnection?, *J. Geophys. Res.*, *109*, A05206, doi:10.1029/2003JA010031.
- Drake, J. F., M. Swisdak, C. Cattell, M. A. Shay, B. N. Rogers, and A. Zeiler (2003), Formation of electron holes and particle energization during magnetic reconnection, *Science*, *299*(5608), 873–877, doi:10.1126/science.1080333.
- Drake, J. F., M. A. Shay, W. Thongthai, and M. Swisdak (2005), Production of energetic electrons during magnetic reconnection, *Phys. Rev. Lett.*, *94*(9), 095001, doi:10.1103/PhysRevLett.94.095001.
- Eastwood, J. P., T.-D. Phan, F. S. Mozer, M. A. Shay, M. Fujimoto, A. Retinò, M. Hesse, A. Balogh, E. A. Lucek, and I. Dandouras (2007), Multi-point observations of the Hall electromagnetic field and secondary island formation during magnetic reconnection, *J. Geophys. Res.*, *112*, A06235, doi:10.1029/2006JA012158.
- Eastwood, J. P., T. D. Phan, M. Øieroset, and M. A. Shay (2010a), Average properties of the magnetic reconnection ion diffusion region in the Earth's magnetotail: The 2001–2005 Cluster observations and comparison with simulations, *J. Geophys. Res.*, *115*, A08215, doi:10.1029/2009JA014962.
- Eastwood, J. P., M. A. Shay, T. D. Phan, and M. Øieroset (2010b), Asymmetry of the ion diffusion region hall electric and magnetic fields during guide field reconnection: Observations and comparison with simulations, *Phys. Rev. Lett.*, *104*(20), 205001, doi:10.1103/PhysRevLett.104.205001.
- Escoubet, C. P., M. Fehringer, and M. Goldstein (2001), The Cluster mission-Introduction, *Ann. Geophys.*, *19*(10-12), 1197–1200, doi:10.5194/angeo-19-1197-2001.
- Fu, X. R., Q. M. Lu, and S. Wang (2006), The process of electron acceleration during collisionless magnetic reconnection, *Phys. Plasmas*, *13*(1), 012309, doi:10.1063/1.2164808.
- Fujimoto, M., M. S. Nakamura, I. Shinohara, T. Nagai, T. Mukai, Y. Saito, T. Yamamoto, and S. Kokubun (1997), Observations of earthward streaming electrons at the trailing boundary of a plasmoid, *Geophys. Res. Lett.*, *24*(22), 2893–2896, doi:10.1029/97GL02821.
- Goldman, M. V., G. Lapenta, D. L. Newman, S. Markidis, and H. Che (2011), Jet deflection by very weak guide fields during magnetic reconnection, *Phys. Rev. Lett.*, *107*(13), 135001, doi:10.1103/PhysRevLett.107.135001.
- Gustafsson, G., et al. (2001), First results of electric field and density observations by Cluster EFW based on initial months of operation, *Ann. Geophys.*, *19*(10-12), 1219–1240, doi:10.5194/angeo-19-1219-2001.
- Hesse, M., M. Kuznetsova, and M. Hoshino (2002), The structure of the dissipation region for component reconnection: Particle simulations, *Geophys. Res. Lett.*, *29*(12), 1563, doi:10.1029/2001GL014714.
- Hoshino, M., T. Mukai, T. Terasawa, and I. Shinohara (2001), Suprathermal electron acceleration in magnetic reconnection, *J. Geophys. Res.*, *106*, 25,979–25,997, doi:10.1029/2001JA900052.
- Huang, C., Q. M. Lu, and S. Wang (2010), The mechanisms of electron acceleration in antiparallel and guide field magnetic reconnection, *Phys. Plasmas*, *17*(7), 072306, doi:10.1063/1.3457930.
- Huang, C., Q. Lu, Z. Yang, M. Wu, Q. Dong, and S. Wang (2011), The evolution of electron current sheet and formation of secondary islands in guide field reconnection, *Nonlinear Processes Geophys.*, *18*, 727–733, doi:10.5194/npg-18-727-2011.
- Huba, J. D. (2005), Hall magnetic reconnection: Guide field dependence, *Phys. Plasmas*, *12*(1), 012322, doi:10.1063/1.1834592.
- Imada, S., R. Nakamura, P. W. Daly, M. Hoshino, W. Baumjohann, S. Muhlbacher, A. Balogh, and H. Rème (2007), Energetic electron acceleration in the downstream reconnection outflow region, *J. Geophys. Res.*, *112*, A03202, doi:10.1029/2006JA011847.
- Johnstone, A., C. Alsop, S. Burge, P. J. Carter, A. J. Coates, A. J. Coker, A. N. Fazakerley, M. Grande, R. A. Gowen, and C. Gurgiolo (1997), PEACE: A plasma electron and current experiments, *Space Sci. Rev.*, *79*(1-2), 351–398, doi:10.1023/A:1004938001388.
- Karimabadi, H., D. Krauss-Varban, N. Omidi, and H. X. Vu (1999), Magnetic structure of the reconnection layer and core field generation in plasmoids, *J. Geophys. Res.*, *104*(A6), 12,313–12,326, doi:10.1029/1999JA900089.
- Karimabadi, H., J. D. Huba, D. Krauss-Varban, and N. Omidi (2004), On the generation and structure of the quadrupole magnetic field in the reconnection process: Comparative simulation study, *Geophys. Res. Lett.*, *31*, L07806, doi:10.1029/2004GL019553.
- Karimabadi, H., W. Daughton, and K. B. Quest (2005), Antiparallel versus component merging at the magnetopause: Current bifurcation and intermittent reconnection, *J. Geophys. Res.*, *110*, A03213, doi:10.1029/2004JA010750.
- Karimabadi, H., W. Daughton, and J. Scudder (2007), Multi-scale structure of the electron diffusion region, *Geophys. Res. Lett.*, *34*, L13104, doi:10.1029/2007GL030306.
- Khotyaintsev, Y. V., A. Vaivads, A. Retino, and M. Andre (2006), Formation of inner structure of a reconnection separatrix region, *Phys. Rev. Lett.*, *97*(20), 205003, doi:10.1103/PhysRevLett.97.205003.
- Lapenta, G., S. Markidis, A. Divin, M. Goldman, and D. Newman (2010), Scales of guide field reconnection at the hydrogen mass ratio, *Phys. Plasmas*, *17*(8), 082106, doi:10.1063/1.3467503.
- Lapenta, G., S. Markidis, A. Divin, M. V. Goldman, and D. L. Newman (2011), Bipolar electric field signatures of reconnection separatrices for a hydrogen plasma at realistic guide fields, *Geophys. Res. Lett.*, *38*, L17104, doi:10.1029/2011GL048572.
- Lennartsson, O. W., L. M. Kistler, and H. Reme (2009), Cluster view of the plasma sheet boundary layer and bursty bulk flow connection, *Ann. Geophys.*, *27*(4), 1729–1741, doi:10.5194/angeo-27-1729-2009.
- Lu, Q., C. Huang, J. Xie, R. Wang, M. Wu, A. Vaivads, and S. Wang (2010), Features of separatrix regions in magnetic reconnection: Comparison of 2-D particle-in-cell simulations and Cluster observations, *J. Geophys. Res.*, *115*, A11208, doi:10.1029/2010JA015713.
- Matsumoto, H., X. H. Deng, H. Kojima, and R. R. Anderson (2003), Observation of Electrostatic Solitary Waves associated with reconnection on the dayside magnetopause boundary, *Geophys. Res. Lett.*, *30*(6), 1326, doi:10.1029/2002GL016319.
- Mozer, F. S., S. D. Bale, and T. D. Phan (2002), Evidence of diffusion regions at a subsolar magnetopause crossing, *Phys. Rev. Lett.*, *89*(1), 015002, doi:10.1103/PhysRevLett.89.015002.
- Nagai, T., I. Shinohara, M. Fujimoto, M. Hoshino, Y. Saito, S. Machida, and T. Mukai (2001), Geotail observations of the Hall current system: Evidence of magnetic reconnection in the magnetotail, *J. Geophys. Res.*, *106*, 25,929–25,949, doi:10.1029/2001JA900038.
- Nagai, T., I. Shinohara, M. Fujimoto, S. Machida, R. Nakamura, Y. Saito, and T. Mukai (2003), Structure of the Hall current system in the vicinity of the magnetic reconnection site, *J. Geophys. Res.*, *108*(A10), 1357, doi:10.1029/2003JA009900.
- Nakamura, R., W. Baumjohann, Y. Asano, A. Runov, A. Balogh, C. J. Owen, A. N. Fazakerley, M. Fujimoto, B. Klecker, and H. Rème (2006), Dynamics of thin current sheets associated with magnetotail reconnection, *J. Geophys. Res.*, *111*, A11206, doi:10.1029/2006JA011706.
- Nakamura, R., et al. (2008), Cluster observations of an ion-scale current sheet in the magnetotail under the presence of a guide field, *J. Geophys. Res.*, *113*, A07S16, doi:10.1029/2007JA012760.
- Øieroset, M., T. D. Phan, M. Fujimoto, R. P. Lin, and R. P. Lepping (2001), In situ detection of collisionless reconnection in the Earth's magnetotail, *Nature*, *412*(6845), 414–417, doi:10.1038/35086520.
- Øieroset, M., R. P. Lin, T. D. Phan, D. E. Larson, and S. D. Bale (2002), Evidence for electron acceleration up to similar to 300 keV in the magnetic reconnection diffusion region of Earth's magnetotail, *Phys. Rev. Lett.*, *89*(19), 195001, doi:10.1103/PhysRevLett.89.195001.
- Phan, T. D., J. F. Drake, M. A. Shay, F. S. Mozer, and J. P. Eastwood (2007), Evidence for an elongated (>60 ion skin depths) electron diffusion region during fast magnetic reconnection, *Phys. Rev. Lett.*, *99*(25), 255002, doi:10.1103/PhysRevLett.99.255002.
- Pritchett, P. L. (2001), Geospace Environment Modeling magnetic reconnection challenge: Simulations with a full particle electromagnetic code, *J. Geophys. Res.*, *106*, 3783–3798, doi:10.1029/1999JA001006.
- Pritchett, P. L. (2005), Onset and saturation of guide-field magnetic reconnection, *Phys. Plasmas*, *12*, 062301, doi:10.1063/1.1914309.
- Pritchett, P. L. (2006), Relativistic electron production during guide field magnetic reconnection, *J. Geophys. Res.*, *111*, A10212, doi:10.1029/2006JA011793.
- Pritchett, P. L., and F. V. Coroniti (2004), Three-dimensional collisionless magnetic reconnection in the presence of a guide field, *J. Geophys. Res.*, *109*, A01220, doi:10.1029/2003JA009999.
- Rème, H., et al. (2001), First multispacecraft ion measurements in and near the Earth's magnetosphere with the identical Cluster ion spectrometry (CIS) experiment, *Ann. Geophys.*, *19*(10–12), 1303–1354, doi:10.5194/angeo-19-1303-2001.
- Retinò, A., et al. (2006), Structure of the separatrix region close to a magnetic reconnection X-line: Cluster observations, *Geophys. Res. Lett.*, *33*, L06101, doi:10.1029/2005GL024650.
- Ricci, P., J. U. Brackbill, W. Daughton, and G. Lapenta (2004), Collisionless magnetic reconnection in the presence of a guide field, *Phys. Plasmas*, *11*(8), 4102–4114, doi:10.1063/1.1768552.
- Robert, P., M. W. Dunlop, A. Roux, and G. Chanteur (1998), Accuracy of current determination, in *Analysis Methods for Multi Spacecraft Data*, edited by G. Paschmann and P. W. Daly, p. 395, Eur. Space Agency, Bern, Switzerland.
- Rogers, B. N., R. E. Denton, and J. F. Drake (2003), Signatures of collisionless magnetic reconnection, *J. Geophys. Res.*, *108*(A3), 1111, doi:10.1029/2002JA009699.

- Runov, A., et al. (2003), Current sheet structure near magnetic X-line observed by Cluster, *Geophys. Res. Lett.*, *30*(11), 1579, doi:10.1029/2002GL016730.
- Russell, C. T., M. M. Mellott, E. J. Smith, and J. H. King (1983), Multiple spacecraft observations of interplanetary shocks: Four spacecraft determination of shock normals, *J. Geophys. Res.*, *88*(A6), 4739–4748, doi:10.1029/JA088iA06p04739.
- Schwartz, S. J. (1998), Schock and discontinuity normals, mach numbers, and related parameters, in *Analysis Methods for Multi Spacecraft Data*, edited by G. Paschmann and P. W. Daly, p. 256, Eur. Space Agency, Bern Switzerland.
- Shay, M. A., J. F. Drake, B. N. Rogers, and R. E. Denton (2001), Alfvénic collisionless magnetic reconnection and the Hall term, *J. Geophys. Res.*, *106*(A3), 3759–3772, doi:10.1029/1999JA001007.
- Shay, M. A., J. F. Drake, and M. Swisdak (2007), Two-scale structure of the electron dissipation region during collisionless magnetic reconnection, *Phys. Rev. Lett.*, *99*(15), 155002, doi:10.1103/PhysRevLett.99.155002.
- Sonnerup, B. U. Ö. (1979), Magnetic field reconnection, in *Solar System Plasma Physics*, edited by L. T. L. C. F. Kennel and E. N. Parker, pp. 45–108, Elsevier, New York.
- Sonnerup, B. U. Ö., and M. Scheible (1998), Minimum and maximum variance analysis, in *Analysis Methods for Multi Spacecraft Data*, edited by G. Paschmann and P. W. Daly, p. 185, Eur. Space Agency, Bern Switzerland.
- Swisdak, M., J. F. Drake, M. A. Shay, and J. G. McIlhargey (2005), Transition from antiparallel to component magnetic reconnection, *J. Geophys. Res.*, *110*, A05210, doi:10.1029/2004JA010748.
- Terasawa, T. (1983), Hall current effect on tearing mode instability, *Geophys. Res. Lett.*, *10*(6), 475–478, doi:10.1029/GL010i006p00475.
- Vaivads, A., et al. (2004), Structure of the magnetic reconnection diffusion region from four-spacecraft observations, *Phys. Rev. Lett.*, *93*, 105001, doi:10.1103/PhysRevLett.93.105001.
- Wang, R. S., Q. M. Lu, J. Guo, and S. Wang (2008), Spatial distribution of energetic electrons during magnetic reconnection, *Chin. Phys. Lett.*, *25*, 3083–3085, doi:10.1088/0256-307X/25/8/093.
- Wang, R. S., Q. M. Lu, C. Huang, and S. Wang (2010a), Multispacecraft observation of electron pitch angle distributions in magnetotail reconnection, *J. Geophys. Res.*, *115*, A01209, doi:10.1029/2009JA014553.
- Wang, R. S., Q. M. Lu, A. M. Du, and S. Wang (2010b), In situ observations of a secondary magnetic island in an ion diffusion region and associated energetic electrons, *Phys. Rev. Lett.*, *104*, 175003, doi:10.1103/PhysRevLett.104.175003.
- Wang, R., Q. Lu, X. Li, C. Huang, and S. Wang (2010c), Observations of energetic electrons up to 200 keV associated with a secondary island near the center of an ion diffusion region: A Cluster case study, *J. Geophys. Res.*, *115*, A11201, doi:10.1029/2010JA015473.
- Wang, Y., F. S. Wei, X. S. Feng, S. H. Zhang, P. B. Zuo, and T. R. Sun (2010), Energetic electrons associated with magnetic reconnection in the magnetic cloud boundary layer, *Phys. Rev. Lett.*, *105*, 195007, doi:10.1103/PhysRevLett.105.195007.